

In-Simulation Testing of Deep Learning Vision Models in Autonomous Robotic Manipulators

Dmytro Humeniuk
Polytechnique Montréal
Montreal, Quebec, Canada
dmytro.humeniuk@polymtl.ca

Thomas Reid
Sycodal
Montreal, Quebec, Canada

Housseem Ben Braiek
Sycodal
Montreal, Quebec, Canada
h.benbraiek@sycodal.ca

Foutse Khomh
Polytechnique Montréal
Montreal, Quebec, Canada

ABSTRACT

Testing autonomous robotic manipulators is challenging due to the complex software interactions between vision and control components. A crucial element of modern robotic manipulators is the deep learning based object detection model. The creation and assessment of this model requires real world data, which can be hard to label and collect, especially when the hardware setup is not available. The current techniques primarily focus on using synthetic data to train deep neural networks (DNNs) and identifying failures through offline or online simulation-based testing. However, the process of exploiting the identified failures to uncover design flaws early on, and leveraging the optimized DNN within the simulation to accelerate the engineering of the DNN for real-world tasks remains unclear. To address these challenges, we propose the MARTENS (Manipulator Robot Testing and Enhancement in Simulation) framework, which integrates a photorealistic NVIDIA Isaac Sim simulator with evolutionary search to identify critical scenarios aiming at improving the deep learning vision model and uncovering system design flaws. Evaluation of two industrial case studies demonstrated that MARTENS effectively reveals robotic manipulator system failures, detecting 25% to 50% more failures with greater diversity compared to random test generation. The model trained and repaired using the MARTENS approach achieved mean average precision (mAP) scores of 0.91 and 0.82 on real-world images with no prior retraining. Further fine-tuning on real-world images for a few epochs (less than 10) increased the mAP to 0.95 and 0.89 for the first and second use cases, respectively. In contrast, a model trained solely on real-world data achieved mAPs of 0.8 and 0.75 for use case 1 and use case 2 after more than 25 epochs.

KEYWORDS

simulation, on-line testing, DNN testing, autonomous robotic manipulators, evolutionary search

ACM Reference Format:

Dmytro Humeniuk, Housseem Ben Braiek, Thomas Reid, and Foutse Khomh. 2024. In-Simulation Testing of Deep Learning Vision Models in Autonomous Robotic Manipulators. In *39th IEEE/ACM International Conference on Automated Software Engineering (ASE '24)*, October 27-November 1, 2024, Sacramento, CA, USA. ACM, New York, NY, USA, 12 pages. <https://doi.org/10.1145/3691620.3695281>

1 INTRODUCTION

Autonomous robotic manipulators (ARMs), also known as robotic arms, play a crucial role in industrial automation, being widely used for tasks such as palletization and machine tending. To perform tasks autonomously, these systems are equipped with various sensors, including cameras and lidars, allowing them to perceive their surroundings. Data from these sensors is processed by software incorporating machine learning components, such as deep neural networks (DNNs), which excel at detecting visual objects in 2D images, making them suitable for robotic guidance applications. However, the performance of these models is heavily dependent on the training data, which is typically collected and annotated manually, a process that is labor-intensive. Moreover, the collected samples may not encompass all edge cases that occur in foreseeable operational conditions. One solution to addressing the limited annotated datasets is the creation of synthetic data. This synthetic data can be initially used to evaluate the model's performance beyond the in-distribution samples. A selection of data points can then be incorporated into the next training set to enhance the model's robustness and generalization abilities.

On one hand, when synthetic data is generated through image transformations [5, 34] or generative models [49], there is no guarantee that it accurately represents naturally occurring use cases. These methods primarily introduce noise and distribution shifts to challenge the model's robustness against alterations in the input data. However, they often fail to produce operational corner cases that reflect specific, adverse environmental conditions. Consequently, while these techniques test the DNN's resilience to input variations, they may not adequately simulate the real-world complexities that the DNN will encounter in practical scenarios. Several methods [2, 11] leverage simulation environments to generate challenging and fault-revealing test inputs for the DNNs that are used to improve the DNN model for predictions in the real world. These works however, only consider the offline test data generation despite numerous studies [16, 40] highlighting the importance of

Permission to make digital or hard copies of all or part of this work for personal or classroom use is granted without fee provided that copies are not made or distributed for profit or commercial advantage and that copies bear this notice and the full citation on the first page. Copyrights for components of this work owned by others than the author(s) must be honored. Abstracting with credit is permitted. To copy otherwise, or republish, to post on servers or to redistribute to lists, requires prior specific permission and/or a fee. Request permissions from permissions@acm.org.

ASE '24, October 27-November 1, 2024, Sacramento, CA, USA

© 2024 Copyright held by the owner/author(s). Publication rights licensed to ACM.

ACM ISBN 979-8-4007-1248-7/24/10

<https://doi.org/10.1145/3691620.3695281>

conducting online testing for autonomous robotic systems with DNN-based components. Indeed, on-line evaluation of DNNs is important as statistical metrics like F1-score and mean Average Precision (mAP) do not allow to capture the failures arising from the DNN interactions with the environment and other system components.

Existing simulation-based testing methods are dedicated either to autonomous driving systems (ADS) [25, 35, 51] or unmanned aerial vehicles (UAVs) [23], with few studies focusing on ARM testing [1]. These methods often aim to expose weaknesses in DNNs by generating adversarial test cases through closed loop simulation of the system but do not propose solutions for repairing the identified failures. Therefore, we identify the need for test generation approaches that include both simulation-based online testing of autonomous robotic systems (ARS) with DNN components, as well as the system improvement from failures. Moreover, when improving the perception system from data collected in simulation, it is important to evaluate the usefulness of the improved system on the real world data.

To address the existing gap in the state-of-the-art approaches for DNN online testing and repair, we propose the MARTENS (Manipulator Robot Testing and Enhancement in Simulation) framework. This framework combines a photorealistic NVIDIA Isaac Sim simulator with evolutionary search for identifying critical scenarios, collecting useful data for system design assessment, testing and improving vision models. Using NVIDIA Isaac Sim, we created a photorealistic simulation environment for ARM applications, enabling the collection of synthetic 2D annotated images for training the DL vision models. The trained DL model is then deployed within the simulation to guide the robot in its manipulation tasks. MARTENS leverages evolutionary search to adjust structural parameters such as object positions and lighting, producing in-simulation tests that reveal failures. These failed test cases provide valuable data for refining the DL model and investigating the limitations of the control and perception strategies. Our evaluation, conducted through two industrial use cases involving pick-and-place tasks, demonstrates that our approach can effectively reveal diverse failures and can be leveraged to repair the DL model. On average, 31% of the generated in-simulation test cases resulted in the ARM failing the task. By fine-tuning the DL models with synthetic images from failed test cases, we achieved a 99% success rate in fixing these issues. A detailed analysis of the non-repaired test cases led to the discovery of some important robotic application design flaws. Finally, MARTENS facilitates the convergence to an optimal vision model using synthetic datasets, providing a pre-trained model that engineers can fine-tune with real-world datasets. An effective sim-to-real model transfer procedure reduces the need for extensive real-world data collection and labelling as well as online testing of the vision model using a real robotic system. We evaluate our model trained with synthetic data on the real world images, matching the scene represented in the simulation environment. The model trained and repaired using the MARTENS approach achieved mean average precision (mAP) scores of 0.91 and 0.82 on real-world images with no prior retraining. Further fine-tuning on real-world images for a few epochs (less than 10) increased the mAP to 0.95 and 0.89 for the first and second use cases (UC-1 and UC-2), respectively. In contrast, a model trained

solely on real-world data achieved mAPs of 0.8 and 0.75 for UC-1 and UC-2 after more than 25 epochs.

The rest of this paper is structured as follows: Section 2 describes the details of MARTENS approach for in-simulation DNN testing and improvement. Evaluation results are presented in Section 3.2. Section 4 discusses the relevant related works, and Section 5 concludes the paper.

2 APPROACH

The overall diagram of the MARTENS approach illustrating the major steps is shown in Figure 1. In this section, we provide a detailed overview of each of the indicated steps.

2.1 In-simulation Test Environment Specification

The first step in testing perception components in the simulation is setting up a photorealistic parametrizable environment. It should mimic the production environment and produce the variability needed for testing the vision system by randomizing parameters. In a typical environment for testing autonomous robotic manipulators, there are objects with fixed position (static objects) O_s , objects with variable position (flexible objects) O_f , a robot R , a light source L and a camera C with a preset angle of view. To create this typical environment within Isaac Sim, the robot R should be imported using its standard format, URDF (Unified Robot Description Format), which is generally provided by the manufacturer. The robot's URDF contains its physical description, including joints, mass, etc. The objects O_s and O_f can be imported to the simulation from their corresponding 3D computer aided design (CAD) models. The light sources and virtual cameras are included within Isaac Sim and can be conveniently configured. Indeed, Isaac Sim features different types of light sources [32] such as rectangular light, distant light, sphere light, cylindrical light, etc. To replicate a conventional lighting condition, we can place the light source L higher in the ceiling and use the rectangular light type that emits a uniform illumination. Varying luminosity is important for testing the robustness of vision models [9].

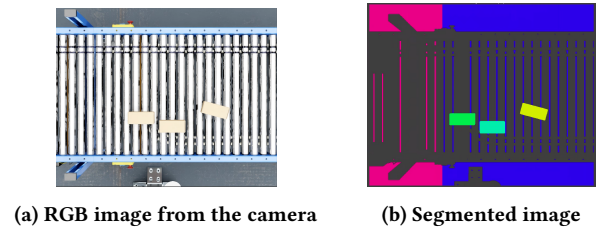


Figure 2: Camera view in the virtual environment

The camera C has a pre-defined angle of view and provides RGB images of the virtual environment that are then processed by the vision system. The camera can be located in a fixed position in the scene, also known as ‘eye-to-hand’ camera or it can be mounted on the robot, known as ‘eye-in-hand’ camera. Figure 2a displays an image captured by an ‘eye-to-hand’ camera mounted on top of the manipulable objects. At inference time, the DL vision predicts

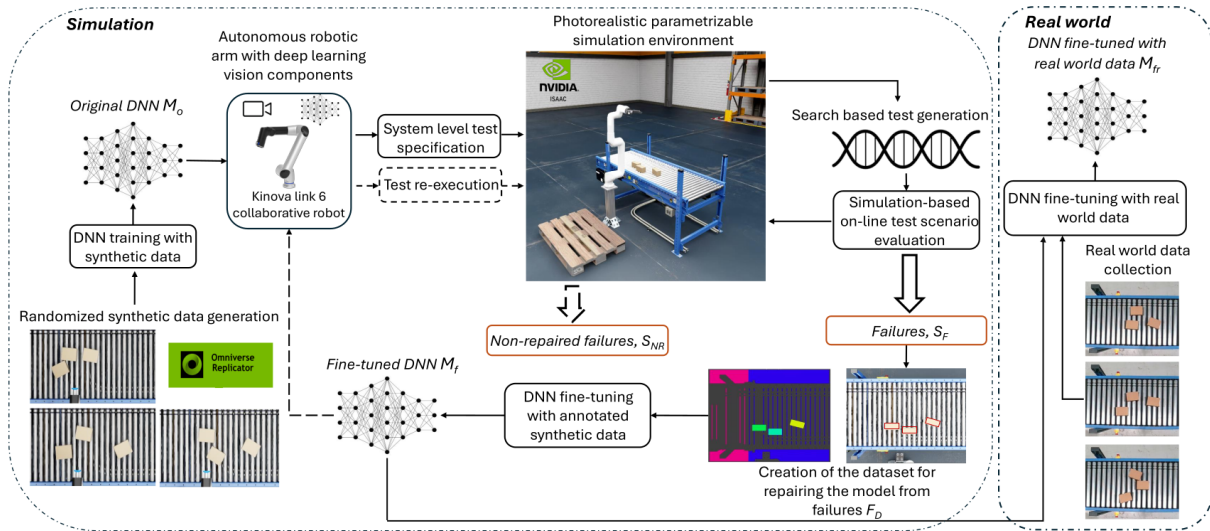


Figure 1: The diagram of the MARTENS approach

the target outputs given the RGB images captured by the virtual camera. However, the estimated pixel coordinates within the 2D images should be projected into the world space of the robot. In real-world production settings, the projection matrix is generally computed using 3D camera calibration [7]. Isaac Sim API provides a function that allows to obtain the coordinates in the world frame from the pixel coordinates in the image. This eliminates the need to calibrate the camera in the simulation and allows for testing the DL vision model with an ideal camera calibration. Moreover, the simulator provides the ground truth information on the position and class of every object in the scene, as shown in Figure 2b.

The ARM R is tasked with a pick and place task of the flexible objects O_f . The ARM should satisfy two requirements while completing the task. The first requirement R_1 is that each placed O_{f_i} should be placed parallel to the palette with no more than ϕ_d degrees of deviation. The second requirement is to perform the placement of each O_{f_i} in the target location. Having set up the test environment in the simulator, we determine the environmental factors that could influence the vision model predictions and the outcomes of the vision-guided robot movements. Given the typical environment of an ARM application described above as well as the system performance requirements, we find that the location and orientation of the flexible objects and the lighting intensity affect the vision model predictions. In order to perform the in-simulation testing, these parameters must be dynamically changed through simulation control logic. In the following, we discuss how these parameters are encoded into a vector to allow searching algorithms to explore the parameter space. The goal of the search is to find such set of parameters that make the ARM falsify the established requirements R_1 and/or R_2 .

2.2 Search-based Test Generation

In simulation, randomizing environmental parameters can help generate valid test cases for evaluating vision-guided robotic systems. Nevertheless, the main purpose of testing is to reveal failures

by which we can identify design flaws, bugs in the software, and DNN inefficiencies. There are many methods to guide the search of environmental parameters towards the failure-revealing regions. Previously, evolutionary algorithm-based approaches were proven effective at test generation for autonomous robotic systems [3, 13]. Below, we provide a more detailed description of the elements of our genetic algorithm (GA) based test generation approach.

Individual representation and sampling. We represent the individuals, or chromosomes, as one-dimensional arrays of size $3n + 1$. It contains the concatenation of the n flexible objects' positions, defined as sub-vectors of $[x_i, y_i, r_i]$, where x_i, y_i is the object position in the 3D space with the z-coordinate fixed at a pre-defined value and r_i is the rotation angle of the object w.r.t z-axis. The rotation angles w.r.t x and y-axis are fixed and set to 0. The last dimension corresponds to the luminosity l level in the scene. We define constraints to delimit the vector space in order to ensure that: (i) no intersection occurs between the objects; (ii) positions of objects are in the camera's field of view. Indeed, our use cases involve pick and place operations of objects on a planar surface with known height (the z-coordinate is constant or can be read from a depth sensor). Hence, (x, y) coordinates and rotation with respect to the z-axis are sufficient to represent the locations and orientations of objects O_f posed on a planar surface.

Fitness function. Fitness function quantifies how well an individual meets the objective, guiding the selection of superior individuals over the generations [10]. Robot movement success or failure is a binary information that leads to a sparse fitness function. A continuous score is more suitable for comparing individuals in a generation. Since the DL vision model detects the objects in the 2D image, we calculate the fitness based on the maximum deviation of the estimated object position by the vision system from the actual object position as well as the maximum deviation of the predicted rotation angle from its associated ground truth. The fitness can be

formulated as follows:

$$F = \frac{w_1}{k_p} \cdot \max_{n \in N} \|p_n - p'_n\| + \frac{w_2}{k_r} \cdot \max_{n \in N} \|r_n - r'_n\|, \quad (1)$$

where N is the total number of objects. Parameter p_n corresponds to the predicted position of the object and p'_n of the ground truth object position. r_n corresponds to the estimated object rotation, while the r'_n is the actual object rotation. The two deviations w.r.t object location and orientation are not conflicting objectives, so we can use a single-objective genetic algorithm [10], rather than a multi-objective one, such as NSGA-II [8]. The coefficients w_1 and w_2 are used to assign weight to objectives. The k_p and k_r coefficients normalize the values of the objectives to be from the same range.

Crossover operator. We are using a one-point crossover operator, which is one of the commonly-used operators [46]. Given a pair of parents the crossover point is randomly determined. At this point, genes (components of the chromosomes) are exchanged. Following the generation of the offspring, a constraint feasibility validation is performed. If the constraint is violated, a low fitness value is assigned to the individual.

Mutation operator. We use two mutation operators: random modification operator M_{rm} and replacement operator M_r . M_{rm} operator choose k arbitrary elements of the chromosome (i.e. genes) and then increases or decreases the value of this gene by 10 %. We vary k from 1 to the chromosome size. M_r operator randomly chooses one object described by a set of (x_i, y_i, r_i) values and replaces them with randomly sampled values. The intuition is to change the position and orientation of one of the objects. At the same time, it is ensured that new object position will not cause collisions with the existing boxes. At each generation, one of the operators M_r or M_{rm} is applied with the probability of p_{mut} .

Duplicate removal. At each iteration, we remove the individuals which have a small deviation between them. We estimate the deviation as the cosine distance D_c [12] and compare it to a prefixed minimum threshold, D_{cth} . If the D_c between the two individuals is less than D_{cth} , one of them is removed.

The described algorithm is used to generate the test cases that are then evaluated in the simulation environment. Tests are considered failed if the robotic system is unable to pick or place the objects properly. In simulation, the obtained system behaviors can be compared to their desired counterparts, and a maximum deviation threshold can be established to separate passed from failed tests. We define the thresholds to identify the system failures in our use cases in Section 3.1. As a baseline for the evolutionary search, we implement random search (RS) to generate test cases by arbitrarily selecting values from the allowable ranges. With proper configuration, GA-based search should outperform RS in terms of the proportion of failures revealed while maintaining diversity among the detected failures. For both competing search strategies, the test generation budget is defined by either the allowable total execution time or the maximum number of evaluations. Moreover, the duplicate removal step is applied to both GA and RS.

2.3 Test Evaluation

Generally, we consider the test failed if at least one of the performance requirements is falsified i.e. the object is not placed correctly

on the pallet (i.e., it is not aligned with the pallet, failing the requirement R_1) or it is not successfully picked and transported to the target position (failing requirement R_2). During the test generation, both passed and failed test cases are saved in the corresponding sets S_P and S_F . As we focus on investigating and repairing the test cases with DNN mispredictions, we further split the failures into two subcategories: (i) *soft* failures, where the DNN prediction was not accurate, leading to a violation of one of the requirements; (ii) *hard* failures, where the DNN prediction was acceptable, but the system failed to satisfy either the requirement R_1 or R_2 . Afterwards, we analyse on characteristics of the failed tests S_F in terms of structural features sparseness (test diversity) and severity sparseness (failure mode diversity). Indeed, we leverage the failure sparseness, S_{av} , a metric proposed in the literature [35], to estimate the diversity by computing the average maximum value of the distance metric between each pair of the failed test cases tc :

$$S_{av} = \frac{\sum_i^N \max_j^N \text{dist}(tc_i, tc_j)}{N} \quad (2)$$

where $N = |S_F|$ is the total number of the failed test cases, and dist is the distance metric. We used the cosine distance metric D_C to compute structural features sparseness, S_{avf} . To evaluate the severity sparseness, we defined five possible failure modes of the system, FM , based on domain knowledge and requirements: incorrect box center predicted by DNN FM_1 , incorrect box orientation predicted by DNN FM_2 , failure to place the box FM_3 , incorrect box orientation at placement FM_4 and robot stuck during the execution FM_5 . For each test case, we collect all the failure modes observed during the pick-and-place of each flexible object, O_f . Then, to evaluate the diversity of failure modes, we use Eq. (2), but with a different distance metric dist . We used the number of the identified unique combinations of the failures modes N_{FM} to estimate the distance between two test cases, thereby computing the severity sparseness, S_{avs} . Intuitively, the more unique combination of failure modes are discovered, the better output behavior coverage is achieved.

2.4 Vision Model with Randomized Synthetic Data

As a simulation platform, we selected Nvidia Isaac Sim, which enables advanced GPU-enabled physics simulations with high photorealism. It includes Isaac Replicator [33] that relies on environmental parameters to provide image metadata information such as depth maps and 2D annotations in the form of color-based segmentation (see Figure2b). For pick-and-place applications using 2D vision, we post-process the segmented images to extract the contours of the objects of interest O_f , then, the polygon coordinates delimiting each object are derived to be added as groundtruth annotations with the RGB images. Using the Isaac Replicator API, we propose generating annotated synthetic images by randomizing environmental parameters within specified distributions. This approach produces scenes with diverse object positions and orientations $(x_i, y_i$ and $r_i)$, as well as varying luminosity levels l . The resulting synthetic dataset enables the vision model to learn and generalize, effectively, improving its ability to accurately detect and position objects under various conditions. Then, after training, the model's performance is evaluated using statistical metrics like

mean Average Precision (mAP) based on synthetic validation data collected the same way as the training dataset. The average of mAP is calculated at varying intersection over union (IoU) thresholds, ranging from 0.50 to 0.95. This offline validation process mirrors how vision engineers assess their models' performance to optimize architecture and hyperparameters. However, achieving a perfect mAP of 1.0 is unlikely to be feasible and can even indicate overfitting. Therefore, testing the vision model in production, integrated with the robotic arm, becomes crucial to verify that the DNN's precision is adequate for ensuring successful picking of the object and placement with correct orientation. In the following sections, we discuss the online evaluation of the ARM with the vision model operating within the above-introduced flexible simulation environment. The proposed in-simulation testing serves to refine the vision model by fine-tuning it on examples with its mispredictions and failures, in addition to uncovering potential design flaws in the vision-based robotic arm system early on.

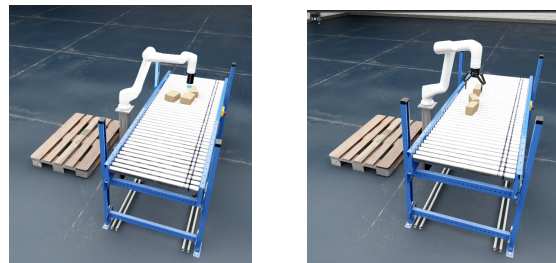
2.5 Model Repair Using Failure Data

The dataset for repairing the DNN model includes all the RGB images of the scene with objects O_f from the camera C , when the ARM failures were detected. For each image, the segmentation data is extracted from the simulator. After post-processing the segmented images, we obtain a dataset D_f of images and labels suitable for model training. This dataset includes all failures identified by the generated test cases, S_f , along with a selection of passed tests from S_p , where the system completed the task but the DNN predictions were inaccurate compared to the ground truth provided by Isaac Sim. Specifically, these are cases where the predicted orientation of the cardboard boxes deviated from the ground truth by more than 5 degrees, or where the predicted center of the boxes deviated by more than 1 cm. These test cases can be categorized as near-fails, denoted S_{NF} . Adding them to our training dataset for fine-tuning can help the model improve its inductive bias and enhance its performance, reducing the likelihood of such cases turning into actual failures. Thanks to transfer learning, the DL vision model does not need to be retrained from scratch on the entire dataset, i.e., combining the original and the novel datasets. Instead, the fine-tuning can be done directly on the last operating model, M_o , considering it as the base (pretrained) model, and fine-tuning it exclusively on the failed dataset, D_f , using the same hyperparameters, except for decreasing the maximum number of epochs. This reduction helps mitigating the risk of catastrophic forgetting phenomenon, where the model overfits to the new samples to the extent of losing its original performance. Furthermore, we use a merged validation dataset that includes original validation data and novel validation data (the collected failed test data). Even with high performance on validation set, offline assessment alone cannot ensure that most of the failures are resolved. It is essential to replay the revealed failures in a subsequent in-simulation testing session using the fine-tuned model M_f . Thus, we re-run the failed test cases from S_f and record a new set of test cases that passed after the model repair S_R ('repaired' test cases) and a set of test cases that did not pass S_{NR} after the repair ('non-repaired' test cases). As a result, we will be able to measure how many failures were fixed by DL vision model repair.

3 EVALUATION

3.1 Experimental Setup

Use cases. We evaluate our approach on two test subjects that are autonomous robotic manipulators performing pick and place task as illustrated in Figure 3. The task aims to automate the process of pulling cardboxes from a conveyor belt and arranging them appropriately on a pallet for delivery. In this task, the robotic manipulators are used for streamlining packaging operations and ensuring efficient transport loading. For both test subjects we use a Kinova link 6 [24] collaborative robot. First test subject (test subject 1) is equipped with suction gripper, while the second subject (test subject 2) with a parallel gripper (Robotiq 2F-85 [37]). Test subject 1 tackles the task of pick and place cardboxes of the 17 x 14 cm size, while the test subject 2 handles the 12 x 8 cm cardboxes. Parallel grippers typically require more precise positioning and control to ensure a successful grasp, than the suction grippers [31]. Both systems have a fixed camera mounted on top of the conveyor belt's region of interest, i.e., reachable by the robot. The camera is an Intel RealSense D435 [21], configured to capture images of the size 640 x 514 pixels.



(a) Manipulator with suction gripper (b) Manipulator with parallel gripper

Figure 3: Illustrations of the test subjects used in the study

The robot needs accurate vision guidance to achieve the grasping of the objects and then complete their proper placement in the pre-defined locations (i.e., properly placed means correct position and orientation). The robot starts in the default position, also known as 'home' position. Then, the image is captured with the fixed camera. If cardboxes are detected by the DL model in the image, the controller initiates the pick and place cycle of the box with the highest detection confidence. The box center coordinates are translated into the robot's coordinate frame and the rotation angle w.r.t the z-axis is sent to the robot to grasp the cardbox with the correct orientation. Once the box is securely grasped, the robot lifts it off the conveyor belt and transports it to the place position. Then, the gripper is opened, box is placed and the robot returns to the home position, where the cycle repeats. When no cardboxes are detected, the controller is stopped. Typically, this cycle is repeated for 3 times as we fixed the number of cardboxes to 3. To implement robot control within Isaac Sim, we used the RMPFlow controller [6], which encapsulates an inverse kinematics solver and enables the implementation of robot primitives for the necessary movements based on computed and vision-estimated positions. When the actual robotic system is implemented, these primitives will be handled

by Kinova’s Kortex API [36]. In both use cases, two operational requirements are defined as follows: R_1 - place the object with a 0-degree orientation relative to the pallet and R_2 - perform the pick and transport the object to the target position. The failure is detected when the box orientation at the place location deviates by more than 5 degrees from the target. Failure is also detected if the box is positioned more than 50% of its size away from the target location.

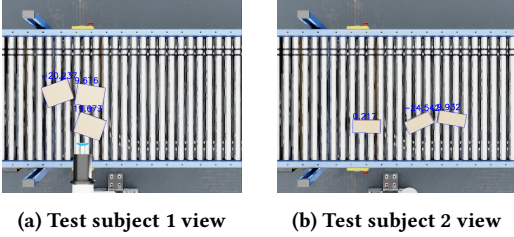


Figure 4: Top views from the fixed camera for the subjects under test with model predictions

Vision models. The vision models are responsible for detecting the positions and orientations of the target objects i.e. cardboxes. An example of the model output predictions are shown in Figure 4. Indeed, the vision system should send the coordinates of the cardbox center and its rotation angle w.r.t the z-axis. This information can be inferred from the 2D images using YOLOv8 [42] that natively supports the oriented bounding box detection. As explained in Section 2.4, images and coordinates of polygons defining cardboxes will be prepared. Such labelled datasets can be used to train YOLOv8 for oriented bounding box detection [43]: its center location, height, width as well as its orientation. For each of the use cases, we trained a dedicated vision DL model using 1200 synthetic images. The images were collected by randomizing the scene parameters through the Isaac Replicator API following the uniform sampling from the ranges shown in Table 1 with the orientation of the boxes ranging from -25 to 25 degrees. We then split the dataset into train set of 960 images and a validation set of 240 images. As recommended by YOLOv8 creators [44], we used a batch size of 16, an adaptive learning rate from 0.01 to 0.0001, and image augmentations like changing the brightness, rotation, scaling, flipping and shear. Using early-stopping on validation data, we trained the models for 100 epochs and both best-fitted models achieved a mean average precision (mAP) of 0.98. Having such high precision is expected since the synthetic dataset is collected using a simulation environment and a uniform sampled data from the same distribution. Online in-simulation testing of the model aims to find inputs that reduce its precision in identifying objects in the scene.

To run the experiments we used ‘g5.2xlarge’ [39] AWS instance with the following characteristics: A10G Tensor Core GPU with 24 Gb of memory, 8 AMD EPYC CPUs, 32 Gb RAM. In comparing the results obtained from the randomized algorithms, we repeated all evaluations at least 5 times due to the computational cost of running the simulations. For all results, we report the non-parametric permutation test [15] with a significance level of $\alpha = 0.05$, as well as the effect size measure in terms of Cliff’s delta [29]. Given the computational constraints to obtain more runs of the algorithms,

we chose permutation test as it makes fewer assumptions about the input data compared to other non-parametric tests such as Mann-Whitney U test [30].

Search algorithm configuration. For both use cases, we fixed the number of flexible objects O_f , i.e. cardboxes, to $N = 3$. The chromosomes are 10-D arrays with the first 9 dimensions representing the positions (x_i, y_i) and rotations (r_i) around the z-axis of the three cardboxes. The last dimension represents the luminosity level l at the scene. The initial population is generated by randomly sampling the values in the allowed ranges, as specified in Table 1. We calculated the fitness function using Eq. (1), with equal weight

Table 1: Allowed ranges for the parameters

x_i	y_i	r_i	l
0.5 – 0.9	0 – 0.92	-30 – 30	1500 – 5000

coefficients w_1 and w_2 set to 0.5. The normalization coefficients k_p and k_r were chosen based on previously recorded values and set to 0.01 and 1, respectively. We fix the value of mutation probability p_{mut} as 0.4, crossover rate p_{cross} as 0.9 and the duplicate removal threshold D_{cth} as 0.1. These values are influenced by our previous studies [20] and confirmed in the warm-up experiments. Population size was set to 40 with the execution budget of 220 evaluations. Over the generations, each individual is used to create the test case scene and evaluate the simulated robotic arm in performing the pick and place of the three cardboxes. The evaluation of each test scene using Isaac Sim is computationally expensive and takes on average 280 seconds for use case 1 (UC-1) and 310 seconds for use case 2 (UC-2) using the GPU-powered AWS instance: ‘g5.2xlarge’. For failure modes, they can be identified as follows: FM_1 occurs when the center O_f predicted by the DNN model deviates from the ground truth by more than 1 cm. FM_2 is noted when the predicted orientation of O_f deviates by more than 5 degrees from the ground truth. FM_3 indicates that O_f was not placed in the target location. FM_4 occurs when the orientation of the placed O_f deviates by more than 5 degrees from the target orientation. FM_5 denotes when the ARM gets stuck during execution and restarts the operation cycle. **Expert feedback.** Given that this research was conducted in partnership with industrial collaborators from Sycodal, we had the opportunity to gather domain expert feedback on each of our research questions (RQs). We conducted two 1-hour interviews with two robotic and vision engineers at Sycodal. During these interviews, we first presented the results obtained for each RQ, followed by a 15-minute discussion. We noted all the points mentioned by the engineers and present them at the end of each RQ.

3.2 Research Questions

3.2.1 RQ1: Effectiveness of MARTENS in revealing ARM failures.

Motivation. We aim to ensure that the designed in-simulation testing method is able to reveal system failures. Our goal is also to determine whether evolutionary search (GA) can reveal more diverse and numerous failures than random search (RS).

Method. For both use cases, we perform five runs of RS and GA with 220 evaluations each. Then, we compute the number of passed versus failed test cases, as well as the near-failed test cases. To distinguish the failure involving DNN prediction inaccuracy and

the system failures even with correct predictions from DNN, we calculate the number of soft versus hard failures. Understanding the failures that occurred when the DNN predictions were adequate is critical as it can point towards some design flows on the control algorithm level. To compare between the GA and RS beyond the number of revealed failures, we measure the structural features sparseness among test environments generated by each method, as well as, the severity sparseness. This gives us the distinctive characteristics among the revealed failures in terms of diversity and coverage.

Table 2: Generated tests statistics for UC-1

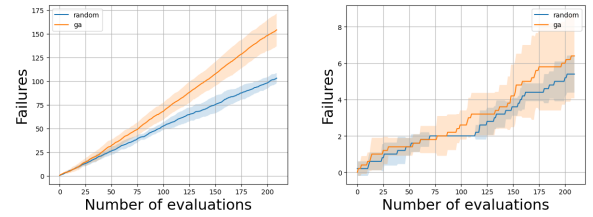
Algorithm	All Tests			Failure Type		Total
	Pass	Fail	Near Fail	Soft	Hard	
RS	531	532	26	510	22	1093
GA	243	794	45	782	12	1082
Total	774	1326	71	1292	34	2175

Table 3: Generated test statistics for UC-2

Algorithm	All Tests			Failure Type		Total
	Pass	Fail	Near Fail	Soft	Hard	
RS	1038	27	33	9	18	1100
GA	935	34	112	12	22	1084
Total	1973	61	145	21	40	2184

Results. Table 2 and Table 3 present all the statistics of passed and failed test cases, as well as their sub-categories for UC-1 and UC-2, respectively. Overall, our approach reveals 1326 and 61 failures in UC-1 and UC-2, respectively, based on more than 2175 generated test cases. Examples of the revealed failing test cases with DNN mispredictions are available online [18]. For the UC-1, the majority of the failures occurred due to model inefficiencies, which affects the precision of vision-based picks and results in 97.4% soft failures. For the UC-2, 65.5 % of the failures are hard, meaning they happened even when the DNN model predicted correctly, suggesting that the pose estimation accuracy needs to be increased or potential design flaws exist. When comparing the numbers obtained by using each searching strategy, we find that GA-driven test generation reveals 50 % (UC-1) and 26 % (UC-2) more failures, than RS-driven test generation. Interestingly, in UC-1 RS reveals more hard failures than RS. We attribute it to the fact that the fitness function is designed to directly promote DNN mispredictions i.e soft failures, rather than the task level failures. Our GA implementation successfully evolves the generations towards being more likely to exploit system vulnerabilities and cause system failures. Figure 5 illustrates the evolution of the number of failures revealed by each strategy over the iterations of the search. Initially, the GA-based test generation begins with random test cases, displaying a similar likelihood of inducing failures as the RS approach. However, over successive iterations, the GA method increasingly exposes more failures compared to RS. This widening gap demonstrates that the GA-based generations are progressively improving. In the following analysis, we compare the structural features and severity sparseness among

the test cases generated by GA and RS to evaluate them in terms of test diversity and failure mode coverage.



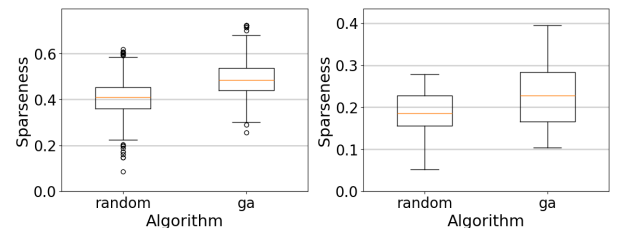
(a) Failure convergence for use case 1 (b) Failure convergence for use case 2

Figure 5: Number of failures revealed over time

Table 4 presents the sparseness metrics obtained by each search strategy, along with the results of the statistical significance tests comparing their differences. As can be seen, GA generates significantly more diverse test cases in terms of structural features compared to RS, with a large effect size. This can also be observed in Figure 6, which displays box plots of feature sparseness values for test cases generated by GA versus RS. Thus, GA not only increases the number of revealed failures by exploiting the characteristics of previous test cases but also enhances the diversity of features among these test cases. The randomness introduced through crossover and mutation in our implementation promotes novelty in new generations, even though they are derived from novelty test cases. In terms of severity sparseness, GA produces higher values than RS; however, there is no statistically significant difference. This indicates that both search strategies were effective in uncovering a variety of failure modes.

Table 4: Sparseness metrics obtained by each search strategy

Use case	Metric	Random	GA	p-value	Effect size
uc1	Features Sparseness	0.406	0.488	< 0.001	-0.563 L
	Severity Sparseness	7.6	7.8	1	-0.12 N
uc2	Features Sparseness	0.188	0.235	0.023	-0.342 M
	Severity Sparseness	2.4	2.8	0.683	-0.28 S



(a) Use case 1 feature sparseness (b) Use case 2 feature sparseness

Figure 6: Sparseness of the structural features of the revealed failures for use cases 1 and 2

Expert feedback. The design of the robot tool and the pick-and-place movements significantly influence the vision system requirements. For the suction gripper use case, containing a big number of soft failures, the precise position and orientation detection play an important role in the task achievement, as most of the task failures occurred following the mispredictions of the DNN model. At the same time, the ARM with parallel gripper in UC-2 is more prone to hard failures. This is because the gripper, being relatively large (when opened), may collide with other objects during the picking or accidentally contact the other cardboard during movement, causing slight deviations from the intended placement position and augmenting the initial errors from the perception module. To compensate for the influence of external factors, the requirements for object detection precision by DNN should be increased.

3.2.2 RQ2: Usefulness of MARTENS in repairing DNN's inefficiencies.

Motivation. We aim to assess the effectiveness of our approach in revealing failures that can be exploited to address inefficiencies in the DNN. We also seek to examine the persistent failures following the DNN repair to understand its limitations and identify potential design flaws.

Method. Based on the obtained failure and near-failures sets S_F and S_{NF} , the DL models are fine-tuned for each use case as described in Section 2.5. To compare the usefulness of our GA implementation with simple RS, we create separate fine-tuned models, M_f^{RS} and M_f^{GA} , which are trained exclusively on datasets collected during the execution of tests generated with their respective search strategies, *RS* and *GA*. Then, we re-run the test cases in the simulation using M_f^{RS} and M_f^{GA} for each use case. We calculate the number of passing, failing, and near-failing tests, noting the type of failures: soft or hard. We refer to the failed tests as 'non-repaired' tests, indicating that the failure persists even with the fine-tuned DNN. To account for the non-determinism of the simulator and ensure these failures are not due to simulator flakiness, we re-run each non-repaired test five times.

Results. Tables 5 and 6 present the statistics on the evaluation of the models fine-tuned with datasets generated by either GA or RS for both use cases.

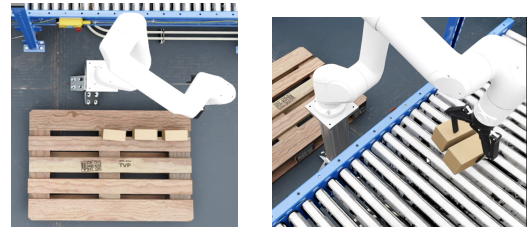
Table 5: UC-1 test analysis after model repair

Algorithm	All Tests			Failure Type		Total
	Pass	Fail	Near Fail	Soft	Hard	
RS	557	1	0	0	1	558
GA	838	1	0	0	1	839
Total	1395	2	0	0	1	1397

Table 6: UC-2 test analysis after model repair

Algorithm	All Tests			Failure Type		Total
	Pass	Fail	Near Fail	Soft	Hard	
RS	59	0	0	0	0	59
GA	145	2	0	0	2	147
Total	204	2	0	0	2	206

For both use cases, most of the failures, more than 99% were successfully repaired, showing that the fine-tuning of the model improves the vision accuracy, so the soft failures are fixed. As expected, the non-repaired tests result from hard failures, indicating instances where the robot failed to complete the task despite accurate cardboard location predictions by the vision model. Interestingly, we observed a reduction in the number of hard failures after repairing the vision model. This improvement underscores the relationship between enhanced precision in pose estimation and increased system robustness, i.e., a more precise vision model can compensate for certain flaws in the robot control design, thereby contributing to improved task completion rates. This reduction of hard failures by vision model repair is aligned with the feedback of experts on the previous RQ results. Given the reduced number of non-repaired tests, we conducted a detailed manual analysis to identify two primary root causes for these hard failures. In both use cases, one recurring issue involved the robot arm shaking before placing the box on top of the pallet, resulting in a misaligned placement. An illustration of such a non-repaired test with a misplaced cardboard box is provided in Figure 7a, with a corresponding video demonstration accessible via the provided link <https://youtu.be/NzXK4LTlnjo>. In addition, for UC-2, the robot was unable to pick objects when the distance between cardboard boxes was too narrow for the parallel gripper to maneuver around the object, as can be seen in Figure 7b and its respective scene video at the link <https://youtu.be/b23gYYBU9cU>.



(a) Robot misplaces the box after shaking. (b) Boxes are too close for the gripper.

Figure 7: Illustration of non-repaired tests

Expert feedback. The generation of failure-revealing test cases is crucial for identifying the design's blind spots and weaknesses. These experiments demonstrate that the suction gripper is generally more suitable than the parallel gripper. As more test cases are simulated, situations arise where the robot cannot perform the pick with the parallel gripper. However, if there is insufficient air pressure for the suction gripper to function properly, several techniques can be implemented to improve the usability of the parallel gripper. For instance, an accelerated conveyor speed can create distance between passing products, or an additional movement can push the product in a certain direction before picking it up if it is in collision with another. Regarding the shaking of the robot, the controller uses Inverse Kinematics (IK) to move the Tool Center Point (TCP) within the Cartesian space. However, this approach is based on numerical optimization, which can be subject to singularity issues, causing the robot to halt its movement. In such situations, the robot controller should move the joints directly without altering the TCP position to escape the singularity and continue the movement.

This issue manifests quickly in the simulator as shaking, which affects the placement accuracy. A possible solution to improve the placement accuracy in this case would be adding a small time delay prior to place allowing the end effector to stabilize.

3.2.3 RQ3: Sim-to-real transferability of the in-simulation optimized DNN.

Motivation. Although our proposed in-simulation testing effectively identifies ARM design flaws and limitations, our primary objective in optimizing the DNN within the simulation is to facilitate its transfer to the real-world with reduced costs.

Method. We collect and label two limited datasets, consisting of approximately 100 images each, from the actual production environments that conform to the simulation for both use cases. First, we evaluate our original DNN trained with synthetic data, denoted M_o , and our optimal, fine-tuned DNN (i.e., obtained by fine-tuning on GA-generated dataset), denoted M_f , for UC-1 and UC-2, on the real-world data. We compute the mean Average Precision (mAP), and incorporate the F1-score to quantify the effects of false negatives (i.e., undetected cardboard boxes) and false positives (i.e., irrelevant regions mistakenly identified as cardboard boxes). We evaluate the models on all the real-world data points. Secondly, we divide the real dataset into training (60%), validation (20%), and testing (20%) subsets, then, we used either M_o or M_f as a pre-trained DNN to train the vision model for detecting cardboard boxes in the real-world environment, referring to the resulting models as M_{or} and M_{of} , respectively. As a baseline, we train a YOLOv8 model using its standard pre-trained weights exclusively on the real-world training dataset, denoted as M_r . We compare the mAP and F1-score of each model on the real world test dataset for each use case, as well as the number of epochs required to converge to the best-fitted model. We consider the model converged if during 5 epochs there is no reduction in loss value. We also report the improvement scores I_{or} and I_{fr} , which compare the relative improvement in percentage for mAP and F_1 scores for the models F_o and F_{or} as well as F_f and F_{fr} . Our intuition is that the performance of the models on the real data should improve as real-world data examples are added to the fine-tuning dataset.

Results. Figure 8 shows the images of the scene set up in the real world. Table 7 reports the mAPs and F1-scores obtained by

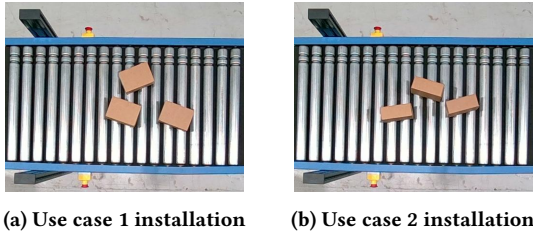


Figure 8: Real-world setups for both use cases

the models, M_o and M_f , on the real-world datasets. For UC-1, both models perform well on the real datasets by having performance metrics higher than 0.9. The fine-tuned model outperforms its original version. As can be seen in Figure 9, M_o fails to detect some cardboard boxes, or detects two colliding ones as the same. For UC-2,

we found similar results, where M_f outperforms M_o , but the overall performance results are substantially lower than the UC-1. As shown in Figure 9, M_o fails to detect some cardboard boxes (i.e., false negatives) while M_f misidentifies irrelevant regions as cardboard boxes (i.e., false positives). Both models struggle to accurately delineate the boundaries of the cardboard boxes, resulting in a lower mAP compared to UC-1. Despite not being trained on real datasets, these models perform relatively well on real images.

Table 7: Performance of the model trained with synthetic data on the real world images

	Use case 1		Use case 2	
	M_o	M_f	M_o	M_f
mAP	0.911	0.915	0.723	0.822
F1	0.962	0.972	0.892	0.93

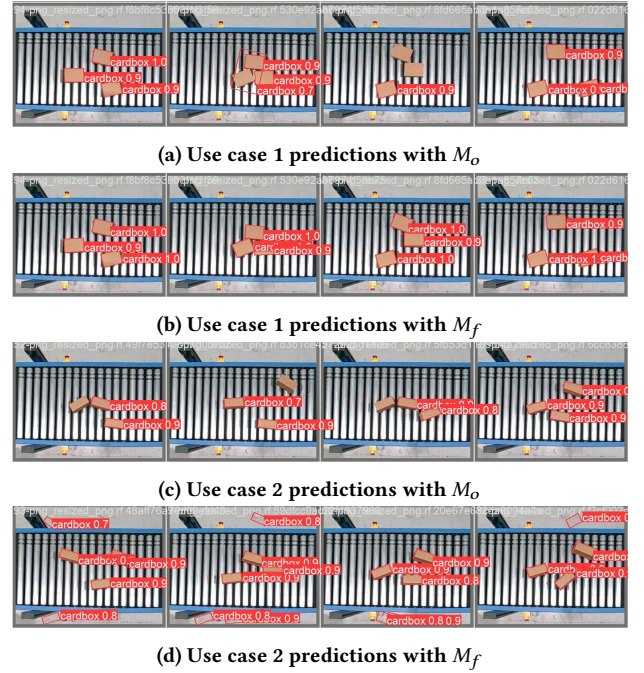


Figure 9: Predictions on the real world data with the models trained on synthetic data for use case 1 and use case 2

Table 8 shows the mAPs, F1-scores, and the number of epochs until convergence for models, M_r , M_{or} and M_{of} . Despite leveraging an established model like YOLOv8 and its built-in features, such as on-the-fly data augmentation, training an acceptable model with a limited real-world dataset proved challenging. This is indicated in the performance metrics obtained for both use cases in Table 8. As introduced in our research work, to achieve better results, a higher investment is necessary to establish an expert-guided protocol for data collection and labelling, ensuring larger real-world datasets with higher coverage for both normal and extreme operating conditions. Notably, for both use cases the fine-tuning on

the real world data improved the mAP score compared to training on only synthetic data as seen from the improvement scores I_{or} and I_{fr} . M_{fr} converged on the real-world fine-tuning dataset of UC-1 after only six epochs of training, whereas M_{or} failed to achieve similar results even with more epochs. Regarding UC-2, M_{fr} outperforms M_{or} in detection performance and M_{or} shows faster convergence. However, further improvements are necessary to develop a production-ready model for UC-2, as M_{fr} could not surpass a 0.9 mAP. Discussions with experts yielded the following feedback.

Table 8: Performance of the model trained on real data without and with pre-trained model on synthetic data

	Use case 1					Use case 2				
	M_r	M_{or}	$I_{or}(\%)$	M_{fr}	$I_{fr}(\%)$	M_r	M_{or}	$I_{or}(\%)$	M_{fr}	$I_{fr}(\%)$
mAP	0.806	0.936	2.7	0.948	3.6	0.755	0.871	20.4	0.892	8.51
F1	0.91	0.968	0.62	0.998	2.67	0.905	0.924	3.58	0.958	3
Epochs	26	9	-	6	-	26	9	-	12	-

Expert feedback. The optimized models in simulation successfully learned relevant inductive biases quickly and efficiently in the production environment. These models were already familiar with the patterns of the cardboxes, the conveyor, and even the colors from the photorealistic simulator (Isaac Sim), as evidenced by their initial performance results on the collected real datasets. Fine-tuning was necessary because of the domain transfer from the simulation to the real world. The models were able to capture the variances of the real domain rapidly, in fewer than 10 epochs, compared to 26 epochs, when no pre-trained model was used. The challenge in solving the real-world version of UC-2 stems from the fisheye effect of the camera. The cardboxes in UC-2 have less width but greater height, creating a fisheye effect that negatively impacts pose estimation by distorting the detection of the box contours. Experts recommend either adjusting the virtual camera parameters in Isaac Sim to simulate a more natural fisheye effect, or modifying the real camera parameters and setup to reduce the fisheye effect on the cardboxes.

4 RELATED WORK

In this section, we discuss the frameworks for testing autonomous robotic systems using simulation. Then, we examine the approaches for improvement of the perception module based on the revealed failures.

4.1 Simulation-based Testing

Several simulation-based testing approaches have been proposed to test end-to-end Autonomous Robotic Systems (ARS) control solutions containing deep learning (DL) components. Examples include DL-driven lane-keeping assist systems tested in the studies by Klikovits et al. [25], Zohdinasab et al. [51], Haq et al. [16], and Riccio et al. [35]. Despite these advancements, implementing end-to-end DL-powered solutions in industrial settings remains challenging. Our approach focuses preliminary on testing DL-based perception components within an ARS containing a separate control module, which is based on a DNN or a traditional control algorithm, such as inverse kinematics (IK) based control. Khatiri

et al. [22] utilized search-based techniques to systematically generate failure-revealing test cases for autonomous unmanned aerial vehicles (UAVs) with obstacle avoidance vision systems. Following the UAV testing competition [23], several new UAV test generation tools were introduced, including TUMB [41], CAMBA [28], WOGAN-UAV [47], DeepHyperion-UAV [50], and AmbieGen [19]. A relatively small number of research works focuses on testing autonomous collaborative robots. Huck et al. [17] leveraged Monte Carlo Tree Search (MCTS) [26] to generate high-risk behavior scenarios in the CoppeliaSim simulator [38]. Their goal was to identify human action sequences that could falsify safety requirements, using traditional robot controllers without DL components. Recently, Adigun et al. [1] developed an evolutionary search strategy for testing ARMs with machine learning-based perception components. However, this and the aforementioned research works focus on generating the failing test cases, without considering the techniques for improving the system under test from the discovered failures.

4.2 DNN Repair

Several techniques have been proposed for repairing DNNs using intelligent data augmentation methods, such as style transfer in DeepRepair [48], search-based data augmentation in SENSEI [14], and image-to-image translation of different environmental conditions in TACTIC [27]. The methods are used in offline mode on 2D images, which can be combined with MARTENS, as we are currently using the on-the-fly augmentation techniques provided by YOLOv8 [45]. It is insufficient to rely solely on 2D image augmentation, and simulation-based test generation is necessary for testing autonomous robotic systems [4]. Attaoui et al. [2] developed the DESIGNATE approach, using generative-adversarial networks (GANs) to transform simulator-generated data into realistic images for DNN retraining. Their evaluation on autonomous driving dataset confirmed its effectiveness compared to models trained only on real-world images. In MARTENS, we use a photorealistic simulator to generate images, avoiding the potential biases introduced by GANs. Additionally, we employ online testing to collect retraining images, rather than relying on static scene specifications as in DESIGNATE.

5 CONCLUSIONS

MARTENS is effective in revealing failures for ARM, allowing the detection of 26% to 50% more failures with higher diversity compared to random test generation. Over 99% of the revealed failures were fixed after fine-tuning the DNN model with data collected from these failures. The remaining failures were attributed to controller misconfiguration or environmental interactions. Following the analysis of these non-repaired tests, engineers proposed three possible design improvements. Using the model repaired with the MARTENS as a pretrained base to perform inference in the real-world environments, we were able to achieve mAPs of 0.948 and 0.892 on test datasets for Use Case 1 and Use Case 2, respectively, after fewer than 10 epochs of fine-tuning. Our future work aims to test the final DNN model on the real robot and develop a method to prioritize and replicate simulation tests for real-world assessment.

REFERENCES

- [1] Jubril Gbolahan Adigun, Tom Philip Huck, Matteo Camilli, and Michael Felderer. 2023. Risk-driven Online Testing and Test Case Diversity Analysis for ML-enabled Critical Systems. In *2023 IEEE 34th International Symposium on Software Reliability Engineering (ISSRE)*. IEEE, 344–354.
- [2] Mohammed Oualid Attaoui, Fabrizio Pastore, and Lionel Briand. 2024. Search-based DNN Testing and Retraining with GAN-enhanced Simulations. *arXiv preprint arXiv:2406.13359* (2024).
- [3] Christian Birchler, Sajad Khatiri, Pouria Derakhshanfar, Sebastiano Panichella, and Annibale Panichella. 2023. Single and multi-objective test cases prioritization for self-driving cars in virtual environments. *ACM Transactions on Software Engineering and Methodology* 32, 2 (2023), 1–30.
- [4] Christian Birchler, Sajad Khatiri, Pooja Rani, Timo Kehrler, and Sebastiano Panichella. 2024. A Roadmap for Simulation-Based Testing of Autonomous Cyber-Physical Systems: Challenges and Future Direction. *arXiv preprint arXiv:2405.01064* (2024).
- [5] Houssein Ben Braiek and Foutse Khomh. 2019. Deepevolution: A search-based testing approach for deep neural networks. In *2019 IEEE International Conference on Software Maintenance and Evolution (ICSME)*. IEEE, 454–458.
- [6] Ching-An Cheng, Mustafa Mukadam, Jan Issac, Stan Birchfield, Dieter Fox, Byron Boots, and Nathan Ratliff. 2020. Rmp flow: A computational graph for automatic motion policy generation. In *Algorithmic Foundations of Robotics XIII: Proceedings of the 13th Workshop on the Algorithmic Foundations of Robotics 13*. Springer, 441–457.
- [7] Peter I Corke, Witold Jachimczyk, and Remo Pillat. 2011. *Robotics, vision and control: fundamental algorithms in MATLAB*. Vol. 73. Springer.
- [8] Kalyanmoy Deb, Amrit Pratap, Sameer Agarwal, and TAMT Meyarivan. 2002. A fast and elitist multiobjective genetic algorithm: NSGA-II. *IEEE transactions on evolutionary computation* 6, 2 (2002), 182–197.
- [9] Hamid Ebad, Mahshid Helali Moghadam, Markus Borg, Gregory Gay, Afonso Fontes, and Kasper Socha. 2021. Efficient and effective generation of test cases for pedestrian detection-search-based software testing of Baidu Apollo in SVL. In *2021 IEEE International Conference on Artificial Intelligence Testing (AITest)*. IEEE, 103–110.
- [10] Agoston E Eiben and James E Smith. 2015. *Introduction to evolutionary computing*. Springer.
- [11] Hazem Fahmy, Fabrizio Pastore, Lionel Briand, and Thomas Stifter. 2023. Simulator-based explanation and debugging of hazard-triggering events in DNN-based safety-critical systems. *ACM Transactions on Software Engineering and Methodology* 32, 4 (2023), 1–47.
- [12] J Foreman. 2014. Cosine Distance, Cosine Similarity, Angular Cosine Distance, Angular Cosine Similarity.
- [13] Alessio Gambi, Marc Mueller, and Gordon Fraser. 2019. Automatically testing self-driving cars with search-based procedural content generation. In *Proceedings of the 28th ACM SIGSOFT International Symposium on Software Testing and Analysis*. 318–328.
- [14] Xiang Gao, Ripon K Saha, Mukul R Prasad, and Abhik Roychoudhury. 2020. Fuzz testing based data augmentation to improve robustness of deep neural networks. In *Proceedings of the acm/ieee 42nd international conference on software engineering*. 1147–1158.
- [15] Phillip Good. 2013. *Permutation tests: a practical guide to resampling methods for testing hypotheses*. Springer Science & Business Media.
- [16] Fitash Ul Haq, Donghwan Shin, Shiva Nejadi, and Lionel C Briand. 2020. Comparing offline and online testing of deep neural networks: An autonomous car case study. In *2020 IEEE 13th International Conference on Software Testing, Validation and Verification (ICST)*. IEEE, 85–95.
- [17] Tom P Huck, Christoph Ledermann, and Torsten Kröger. 2020. Simulation-based testing for early safety-validation of robot systems. In *2020 IEEE Symposium on Product Compliance Engineering-(SPCE Portland)*. IEEE, 1–6.
- [18] Dmytro Humeniuk. 2024. MARTENS framework: examples of DNN mispredictions discovered for the two use cases. <https://doi.org/10.5281/zenodo.12748885>
- [19] Dmytro Humeniuk and Foutse Khomh. 2024. AmbieGen at the SBFT 2024 Tool Competition - CPS-UAV Track. In *IEEE/ACM International Workshop on Search-Based and Fuzz Testing, SBFT@ICSE 2024*.
- [20] Dmytro Humeniuk, Foutse Khomh, and Giuliano Antoniol. 2022. A search-based framework for automatic generation of testing environments for cyber-physical systems. *Information and Software Technology* 149 (2022), 106936.
- [21] Intel. 2023. Intel RealSense Depth Camera D435. <https://www.intelrealsense.com/depth-camera-d435/> Accessed: 2024-07-15.
- [22] Sajad Khatiri, Sebastiano Panichella, and Paolo Tonella. 2023. Simulation-based test case generation for unmanned aerial vehicles in the neighborhood of real flights. In *2023 IEEE Conference on Software Testing, Verification and Validation (ICST)*. IEEE, 281–292.
- [23] Sajad Khatiri, Prasun Saurabh, Timothy Zimmermann, Charith Munasinghe, Christian Birchler, and Sebastiano Panichella. 2024. SBFT tool competition 2024: CPS-UAV test case generation track. In *17th International Workshop on Search-Based and Fuzz Testing (SBFT), Lisbon, Portugal, 14-20 April 2024*. ZHAW Zürcher Hochschule für Angewandte Wissenschaften.
- [24] KINOVA. 2024-01-17. *Kinova link6*. <https://www.kinovarobotics.com/product/link-6-cobot>
- [25] Stefan Klikovits, Ezequiel Castellano, Ahmet Cetinkaya, and Paolo Arcaini. 2023. Frenetic-lib: An extensible framework for search-based generation of robot structures for ADS testing. *Science of Computer Programming* 230 (2023), 102996.
- [26] Ritchie Lee, Ole J Mengshoel, Anshu Saxena, Ryan W Gardner, Daniel Genin, Joshua Silbermann, Michael Owen, and Mykel J Kochenderfer. 2020. Adaptive stress testing: Finding likely failure events with reinforcement learning. *Journal of Artificial Intelligence Research* 69 (2020), 1165–1201.
- [27] Zhong Li, Minxue Pan, Tian Zhang, and Xuandong Li. 2021. Testing dnn-based autonomous driving systems under critical environmental conditions. In *International Conference on Machine Learning*. PMLR, 6471–6482.
- [28] Marco De Liso and Zhi Wen Soi. 2024. CAMBA CPS-UAV at the SBFT Tool Competition 2024. In *IEEE/ACM International Workshop on Search-Based and Fuzz Testing, SBFT@ICSE 2024*.
- [29] Guillermo Macbeth, Eugenia Razumiejczyk, and Rubén Daniel Ledesma. 2011. Cliff’s Delta Calculator: A non-parametric effect size program for two groups of observations. *Universitas Psychologica* 10, 2 (2011), 545–555.
- [30] Henry B Mann and Donald R Whitney. 1947. On a test of whether one of two random variables is stochastically larger than the other. *The annals of mathematical statistics* (1947), 50–60.
- [31] Gareth J Monkman, Stefan Hesse, Ralf Steinmann, and Henrik Schunk. 2007. *Robot grippers*. John Wiley & Sons.
- [32] NVIDIA. 2022. Different Types of Light Sources in NVIDIA Isaac Sim. https://omniverse-content-production.s3-us-west-2.amazonaws.com/Assets/Isaac/Documentation/Isaac-Sim-Docs_2022.2.1/materials-and-rendering/latest/103/lighting.html Accessed: 2024-07-15.
- [33] NVIDIA. 2023. Omniverse Replicator API Documentation. <https://docs.omniverse.nvidia.com/py/replicator/1.5.1/source/extensions/omni.replicator.core/docs/APL.html> Accessed: 2024-07-15.
- [34] Kexin Pei, Yinzhi Cao, Junfeng Yang, and Suman Jana. 2017. Deepxplore: Automated whitebox testing of deep learning systems. In *proceedings of the 26th Symposium on Operating Systems Principles*. 1–18.
- [35] Vincenzo Riccio and Paolo Tonella. 2020. Model-based exploration of the frontier of behaviours for deep learning system testing. In *Proceedings of the 28th ACM Joint Meeting on European Software Engineering Conference and Symposium on the Foundations of Software Engineering*. 876–888.
- [36] Kinova Robotics. 2023. Kinova Kortex API Documentation. <https://docs.kinovarobotics.com/> Accessed: 2024-07-15.
- [37] Robotiq. 2023. 2F-85 and 2F-140 Adaptive Robot Grippers. <https://robotiq.com/products/2f85-140-adaptive-robot-gripper> Accessed: 2024-07-15.
- [38] Eric Rohmer, Surya PN Singh, and Marc Freese. 2013. V-REP: A versatile and scalable robot simulation framework. In *2013 IEEE/RSJ international conference on intelligent robots and systems*. IEEE, 1321–1326.
- [39] Amazon Web Services. 2023. Amazon EC2 Instance Types - G5 Instances. <https://aws.amazon.com/ec2/instance-types/g5/> Accessed: 2024-07-15.
- [40] Andrea Stocco, Brian Pulfer, and Paolo Tonella. 2023. Model vs system level testing of autonomous driving systems: a replication and extension study. *Empirical Software Engineering* 28, 3 (2023), 73.
- [41] Shuncheng Tang, Zhenya Zhang, Ahmet Cetinkaya, and Paolo Arcaini. 2024. TUMB at the SBFT 2024 Tool Competition – CPS-UAV Test Case Generation Track. In *IEEE/ACM International Workshop on Search-Based and Fuzz Testing, SBFT@ICSE 2024*.
- [42] Ultralytics. 2023. YOLOv8. <https://yolov8.com/> Accessed: 2024-07-15.
- [43] Ultralytics. 2023. YOLOv8: Oriented Bounding Boxes. [https://yolov8.com/](https://yolov8.com/Accessed: 2024-07-15) Accessed: 2024-07-15.
- [44] Ultralytics. 2023. YOLOv8 Training Documentation. <https://docs.ultralytics.com/modes/train/> Accessed: 2024-07-15.
- [45] Ultralytics. 2024. Data Augmentation in Ultralytics Framework. <https://docs.ultralytics.com/reference/data/augment/> Accessed: 2024-07-16.
- [46] Anant J Umbarkar and Pranali D Sheth. 2015. Crossover operators in genetic algorithms: a review. *ICTACT journal on soft computing* 6, 1 (2015).
- [47] Jesper Winsten, Valentin Soloviev Jarkko Peltomäki, and Ivan Porres. 2024. Adaptive test generation for unmanned aerial vehicles using WOGAN-UAV. In *IEEE/ACM International Workshop on Search-Based and Fuzz Testing, SBFT@ICSE 2024*.
- [48] Bing Yu, Hua Qi, Qing Guo, Felix Juefei-Xu, Xiaofei Xie, Lei Ma, and Jianjun Zhao. 2021. Deeprepair: Style-guided repairing for deep neural networks in the real-world operational environment. *IEEE Transactions on Reliability* 71, 4 (2021), 1401–1416.
- [49] Mengshi Zhang, Yuqun Zhang, Lingming Zhang, Cong Liu, and Sarfraz Khurshid. 2018. DeepRoad: GAN-based metamorphic testing and input validation framework for autonomous driving systems. In *Proceedings of the 33rd ACM/IEEE international conference on automated software engineering*. 132–142.
- [50] Tahereh Zohdinasab and Andrea Doreste. 2024. DeepHyperion-UAV at the SBFT 2024 Tool Competition - CPS-UAV Test Case Generation Track. In *IEEE/ACM International Workshop on Search-Based and Fuzz Testing, SBFT@ICSE 2024*.

- [51] Tahereh Zohdinasab, Vincenzo Riccio, Alessio Gambi, and Paolo Tonella. 2021. Deephyperion: exploring the feature space of deep learning-based systems through illumination search. In *Proceedings of the 30th ACM SIGSOFT International Symposium on Software Testing and Analysis*. 79–90.